Impact-collision ion-scattering-spectrometry study of Ni layers deposited on Si(111) at room temperature

T. L. Porter, C. S. Chang, U. Knipping, and I. S. T. Tsong
Department of Physics, Arizona State University, Tempe, Arizona 85287
(Received 26 May 1987)

Overlayers of Ni, ranging in thickness from 0.1 to 34 Å, were deposited on a Si(111) surface. Surface structure and composition were monitored during the film growth using impact-collision ion-scattering spectrometry. Results indicate that at extremely low Ni coverages, ~0.1 Å, Ni atoms diffuse into the Si substrate and form regions of predominantly type-*B* $NiSi_2$. Further Ni deposition results in the lateral growth of silicide islands enriched with Si on the surface. At 12 Å coverage the islands coalesce, then grow in thickness until 30 Å Ni has been deposited, at which point a pure-Ni film begins to form.

I. INTRODUCTION

When Ni atoms are deposited onto a clean Si surface at room temperature, the problem of how the initial reaction and film growth proceed is of great interest, since these processes may play an important role in determining subsequent properties such as the structure of epitaxial layers, electronic properties of the interface, and compound formation. Studies by various research groups have attempted to provide answers to this particular problem of initial stages of deposition. X-ray photoemission spectroscopy (XPS) studies by Grunthaner *et al.*[1] show evidence for Ni atoms diffusing into interstitial sites in the Si substrate. Surface extended x-ray-absorption fine-structure (SEXAFS) measurements by Comin *et al.*[2] indicate that Ni atoms diffuse into type-*B* $NiSi_2$ lattice locations. Ion-channeling experiments by Cheung and co-workers[3] and ultraviolet photoemission spectroscopy (UPS) measurements by Chang and co-workers[4] show that Ni atoms occupy tetrahedral interstitial voids in the Si lattice. For higher Ni coverages, ion-channeling studies by Cheung *et al.*[5] show that the Ni-Si room-temperature reaction continues for Ni coverages up to about 35 Å, while medium-energy ion-scattering studies by Van Loenen and co-workers[6] show that the room-temperature Ni-Si reaction stops at a thickness of ~9 Å coverage, after which pure-Ni overlayers form.

In this paper the extreme surface sensitivity of low-energy ion scattering[7] was utilized to monitor the composition of the topmost layer during Ni depositions on Si, allowing us to accurately determine the point at which the Ni-Si reaction stopped and pure-Ni layers began to form. In addition, we used impact-collision ion-scattering spectrometry[8] (ICISS) to obtain structural information concerning the specific lattice sites occupied by the Ni atoms at extremely low coverages.

II. EXPERIMENTAL PROCEDURE

The experiments were carried out in an ultrahigh-vacuum (UHV) chamber fitted with a Colutron ion source as shown in Fig. 1. The lower section of the chamber is equipped with a four-grid reverse-view low-energy electron diffraction–Auger electron spectroscopy (LEED-AES) system, a hemispherical electrostatic energy analyzer (ESA) mounted on a turntable for scattering angles of 0° to 140° for conventional ISS and forward recoil measurements, and a cylindrical ESA fixed in position at a scattering angle of 163° for ICISS measurements. The He^+ ion current at 1 keV could be varied from ~20 nA into a 1-mm-diam spot to 80 nA in a 2-mm spot by selection of appropriate apertures in the beam line. The upper section of the main chamber contains an electron-beam evaporator for thin-film deposition and a crystal thickness monitor. The base pressure of the chamber was typically 1×10^{-10} torr. Target samples were mounted on a precision manipulator allowing *X*, *Y*, and *Z* translations as well as polar and azimuthal rotations. The manipulator was equipped with electron-beam heating and liquid-nitrogen cooling for the sample. The sample holder itself was electrically isolated from the rest of the manipulator via sapphire rings. An *n*-type polished Si(111) wafer with 0.02 Ω cm resistivity and dimensions of 6×5 mm^2 was used. The sample was rinsed in methanol and distilled water prior to a 10-sec etch in a buffered etching solution to remove the native oxide layer. It was then rinsed again in distilled water prior to insertion in the chamber. The surface was sputtered by Ar^+ ions and annealed to 1000 °C for 2 min, followed by slow cooling to room temperature. Such treatment produced consistently sharp 7×7 LEED patterns. The surface orientations derived from the LEED patterns were used to align the sample with respect to the incident ion beam in polar and azimuthal directions.

Nickel was initially deposited on the Si substrate at a rate of approximately 0.1 Å/min; subsequently the thickness was allowed to grow in increments ranging from 0.1 to 4.0 Å (1 Å of Ni corresponds to about 1.2 monolayers on Si, or an areal density of 9.1×10^{14} atoms/cm^2). The uncertainty of the thickness measurement by the crystal monitor was estimated to be within 10%, which should not significantly affect the results.

 ©1987 The American Physical Society

The surface composition was monitored between each deposition by performing an energy scan of the 163° scattered ions, using a 1-keV He^+ beam at normal incidence. Polar scans in the ICISS mode were made between depositions by rotating the sample from 0° incident angle (beam parallel to the surface) to 50° incidence in 2° increments and counting the ions backscattered from either Ni or Si with the cylindrical ESA. For the first few Ni depositions, LEED patterns were also monitored as a check on surface order.

III. RESULTS AND DISCUSSION

A. LEED

After annealing the Si(111) sample at 1000 °C for 2 min and then cooling at 2 °C per second to room temperature, sharp 7×7 LEED patterns were observed. Approximately 0.1 Å Ni was then evaporated onto the surface, with the chamber pressure remaining below 8×10^{-10} torr during deposition. The observed LEED pattern showed the same symmetry as the clean Si surface, but about 60% of the seventh-order spots were extinguished. Most of the integral-order spots remained. An increase in background intensity of about 50% was also observed. This change from the 7×7 pattern to an α-7×7 pattern at submonolayer coverages of Ni has been observed previously,[9] and is most likely due to diffusion of the Ni atoms into atomic sites below the Si surface, with some surface order remaining. Further deposition of Ni up to 0.5 Å coverage yielded LEED patterns with no seventh-order spots remaining and only

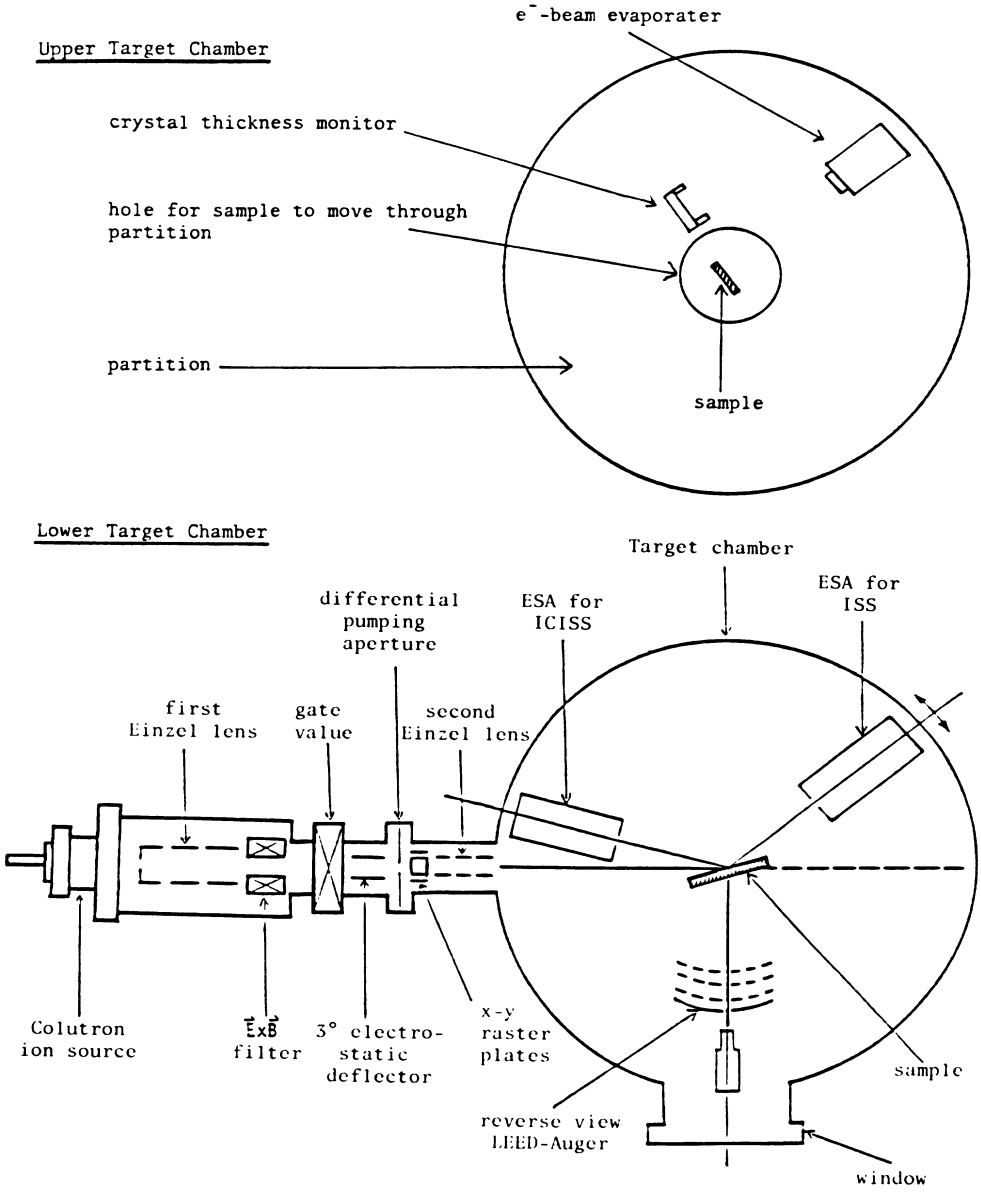

FIG. 1. Schematic diagram of experimental apparatus.

about 50% of the integral-order spots. At 1.0 Å coverage, 80% of the integral-order spots were extinguished, and the background intensity increased. At this point the surface was largely disordered. At 2.0 Å coverage only widely scattered LEED spots were distinguishable from the background, and at 3.0 Å coverage, the LEED pattern disappeared completely, in agreement with a previous observation by Tung *et al.*[10]

B. Surface composition

Results of scattered ion energy scans for Si after each deposition are shown in Fig. 2, and those for Ni are shown in Fig. 3. In both figures, the number of ions singly scattered off Si or Ni atoms at an angle of 163° for a normal incidence 1-keV He^+ primary beam is plotted as a function of Ni coverage. Studies have shown that for low-energy noble-gas ions, the probability of neutralization for ions penetrating below the topmost layer in a close-packed surface is essentially unity.[11–13] Atoms in second- or even third-layer positions can be detected only if the incoming and outgoing trajectories are well clear of overlaying atoms. From Fig. 2 we see that the Si count rate actually increases slowly from 0 to 12 Å Ni coverage. This implies that in this range of coverage, the Ni atoms do not reside on the topmost layer but diffuse into the Si substrate, leaving a Si layer on top. The Si surface becomes at least partially disordered, exposing more Si atoms to the primary beam and giving rise to the slow increase in the Si count rate. Beyond 12 Å Ni coverage the Si count rate begins to drop to the same level observed for a clean Si surface, where it remains until ~30 Å coverage. After 30 Å of deposited Ni, the Si count rate gradually falls to zero, indicating a pure Ni film begins to form on the surface. A similar strong room-temperature reaction for Ni on Si was reported by Van Loenen and co-workers.[6] In that study, medium-energy ion-scattering data indicate increased Ni coverage results in the lateral growth of islands that are

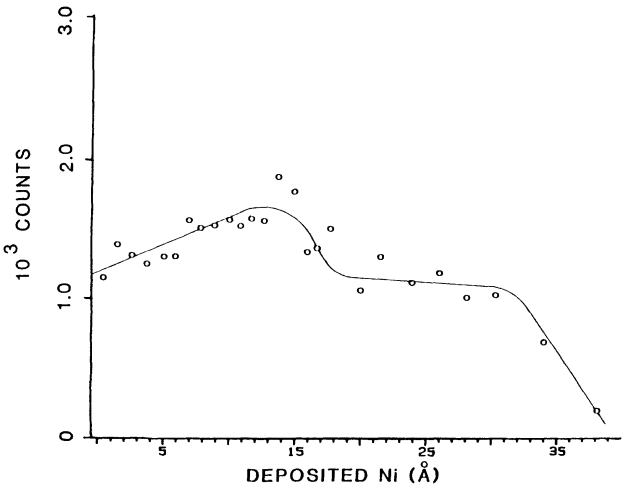

FIG. 2. Counts for 1-keV He^+ ions backscattered from surface Si atoms as a function of Ni coverage. Each data point represents the integral number of counts taken under the Si scattered peak at 562 eV. A top layer of Si atoms remains until approximately 30 Å Ni coverage.

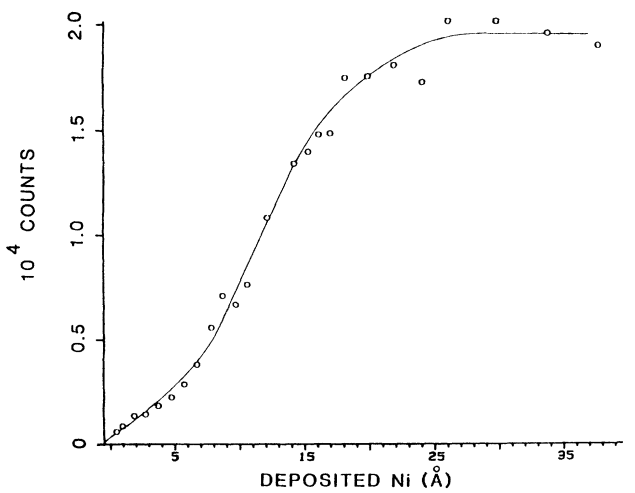

FIG. 3. Counts for 1-keV He^+ ions backscattered from Ni atoms as a function of Ni coverage. Each data point represents the integral number of counts taken under the Ni scattered peak at 760 eV. Saturation occurs at approximately 30 Å coverage.

enriched with Si on the surface, which coalesce at about 9 Å coverage. Results of Ni deposition much beyond this point were not reported. Our Fig. 2 supports that part of the island-growth model in which initially arriving Ni atoms form clusters that grow out laterally as the Ni coverage increases. The Ni atoms arriving initially at the surface react strongly with the Si substrate, diffusing below the surface and leaving a partially disordered Si surface. At about 12 Å coverage, the islands coalesce to form a continuous film as evident from the drop of Si counts. Further Ni deposition, however, shows that Ni atoms continue to diffuse below the Si top layer as the film thickness increases as seen in the plateau of Si counts between 17 and 30 Å. The room-temperature Ni-Si reaction continues until ~30 Å Ni has been deposited, at which point pure Ni layers begin to form on the surface as can be seen by the drop of Si counts in Fig. 2 and saturation of the Ni count rate near 30 Å in Fig. 3.

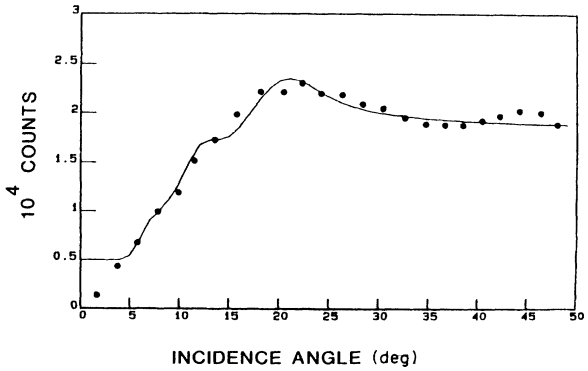

FIG. 4. ICISS polar-angle scan for Ni (solid circles) taken after 0.1 Å Ni deposition. Primary beam of 1-keV He^+ ions is incident along the $[\bar{1}10]$ azimuth. The computer simulation of the backscattered intensity is shown as the solid line.

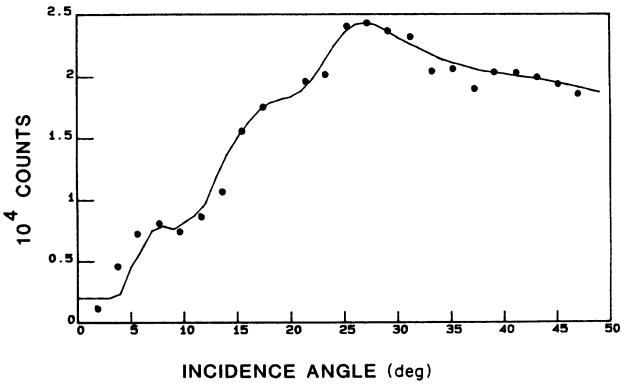

FIG. 5. ICISS polar-angle scan for Ni (solid circles) taken after 0.1 Å Ni deposition. Primary beam incident along the $[\bar{1}\,\bar{1}\,2]$ azimuth. The computer-simulated backscattered intensity is shown as a solid line.

C. Surface structure

ICISS polar scans were taken with the scattered energy set on the Ni peak for 1-keV He^+ ions. Scans taken with the primary beam incident along the $[\bar{1}10]$ and $[\bar{1}\,\bar{1}\,2]$ azimuths after deposition of 0.1 Å Ni are shown in Figs. 4 and 5, respectively. The $[\bar{1}10]$ polar scan shows a peak at 19° (Fig. 4) for the backscattered flux from Ni, while the $[\bar{1}\,\bar{1}\,2]$ scan shows a large peak at about 26°. The $NiSi_2$ type-*B* surface along the $[\bar{1}10]$ direction consists of alternating rows of Si and Ni atoms,[10] with the Ni rows ~0.7 Å below the Si rows (Fig. 6). The spacing between the Ni atoms in the $[\bar{1}10]$ direction is ~3.82 Å.[14] If we use a shadow cone radius of 1.2 Å for this case,[15] the critical angle at which the shadow cone envelope just passes through adjacent Ni atoms is calculated to be 18°. Along the $[\bar{1}\,\bar{1}\,2]$ direction, Ni atoms are initially shadowed by Si atoms 0.74 Å above and 4.43 Å away. Using a shadow cone radius of 1.1 Å (Ref. 15) for this case, the critical angle is calculated to be 24°. The agreement between calculated and experimental values for the critical angles suggests that at extremely low Ni coverages, Ni atoms tend to diffuse into the Si substrate at room temperature to form areas of type-*B* $NiSi_2$. A computer simulation based on an $NiSi_2$ surface was then used to identify the secondary flux peaks in the $[\bar{1}10]$ and $[\bar{1}\,\bar{1}\,2]$ scans.

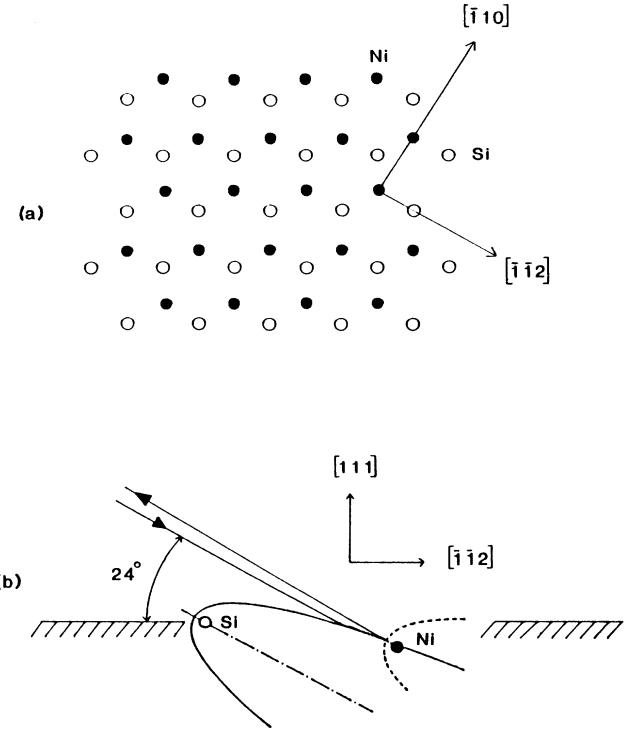

FIG. 6. Model of the type-*B* $NiSi_2$ surface. Only top-layer Si atoms (open circles) and second-layer Ni atoms (solid circles) are shown. Vertical spacing between the top two layers is 0.74 Å. (a) Top view of surface. (b) Side view showing the onset of shadowing at the critical angle in the $[\bar{1}\,\bar{1}\,2]$ azimuth.

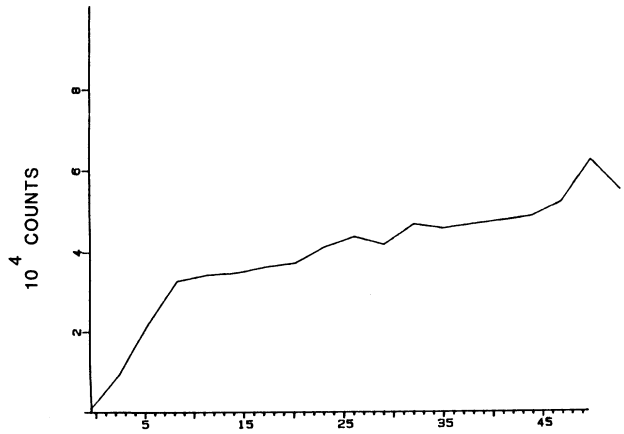

FIG. 7. ICISS polar-angle scan for Ni taken after 3 Å Ni coverage. Primary beam incident along the $[\bar{1}10]$ azimuth. All polar scans taken from 0.3 to 5.0 Å Ni coverage in both $[\bar{1}10]$ and $[\bar{1}\,\bar{1}\,2]$ azimuths display the same structure.

Computer simulation of the scattering process was made using the two-atom model of Yarmoff *et al.*[16] The deflection angles were calculated using the Thomas-Fermi-Moliere potential with a screening length scaling factor of 0.9.[15] For ICISS, the blocking effect is negligible, and was not considered. Simulation of the shadowing effect was made by calculating the scattering cross section (two-atom model), taking into account thermal vibrations and neutralization effects. Vibrational amplitudes of 0.13 and 0.15 Å were used for the surface Ni and Si atoms, respectively (1.4 times their bulk values).[17] The characteristic velocities of neutralization used for Ni in the $[\bar{1}10]$ and $[\bar{1}\,\bar{1}\,2]$ azimuths were 1.6×10^7 and 2.9×10^7 cm/s, respectively, which are slightly smaller than those proposed by Brongersma and Buck.[18] Because of the extremely high neutralization rate for noble-gas ions, only the top two layers were used in the simulations. Results of the simulations are plotted along with the experimental data in Figs. 4 and 5. For the perfect $NiSi_2$ surface, we expect ICISS flux peaks at only 21° for the $[\bar{1}10]$ azimuth and 27° for the $[\bar{1}\,\bar{1}\,2]$ azimuth, if

only the first two $NiSi_2$ layers are considered. For an Ni coverage as low as 0.1 Å, however, we must take into account the large number of available vacant sites. While our data shows the Ni atoms locating in the predominantly type-*B* lattice sites, a small percentage may occupy type-*A* sites as well. Ni atoms occupying random or other lattice sites were not considered. The computer simulation for scattering in the $[\bar{1}10]$ direction (Fig. 4) was made by combining results for various possible vacancy combinations. The spacing between two adjacent Ni atoms in the $[\bar{1}10]$ direction for a perfect $NiSi_2$ surface is $d=3.82$ Å (Fig. 6). A single vacancy in the $[\bar{1}10]$ direction would result in a spacing of $2d$. The relative concentrations of vacancies used for the simulation was d, 33%; $2d$, 27%; $3d$, 10%; $4d$, 10%; $>4d$, 20%. This combination resulted in the best fit to experimental data. The small shoulders at 7°, 10°, and 13° in the computer simulation (Fig. 4) correspond to the $4d$, $3d$, and $2d$ vacancies, respectively. The computer simulation begins at 4° incident angle in Fig. 4 rather than 0° because we did not further simulate any separate vacancy spacings from $5d$ onwards. Type-*A* lattice locations for Ni along the $[\bar{1}10]$ direction are the same as type *B*, so for the simulation in Fig. 4 we did not need to consider any presence of type-*A* structure.

For scattering the $[\bar{1}\,\bar{1}\,2]$ direction, the Ni atoms are situated 0.74 Å below the top Si layer [Fig. 6(b)]. The spacing between two adjacent Si atoms and that between two adjacent Ni atoms are both given by $d=6.65$ Å. In the type-*B* configuration, the Ni atom is 4.43 Å away from the Si atom; while in the type-*A* configuration, it is 2.22 Å away from the Si atom. Computer simulation using only type-*B* lattice locations and their associated vacancies for the Ni and Si atoms could not account for the observed shoulders in the experimental data at 17° and 42°. If, however, we take into account type-*A* occupancy and assume that we have 75% type-*B* and 25% type-*A* $NiSi_2$, the fit to experimental data was good (Fig. 5). The simulated curve in Fig. 5 begins at incident angle 3° rather than 0° since we only consider separate vacancy spacings up to $3d$.

Polar scans for Ni taken at coverages of 0.3 to 5.0 Å show a different behavior. The backscattered intensity in both $[\bar{1}10]$ and $[\bar{1}\,\bar{1}\,2]$ directions show a very steep rise in the range 0° (glancing incidence) to 7°, followed by a gradual leveling off (Fig. 7). Lattice location information on the Ni atoms is lost, either by the random shadowing effects of the growing silicide islands, or by the surface becoming mostly disordered as the Ni coverage increases. The steep initial rise in the backscattered intensity observed in this range of coverage is most likely due to the edges of the silicide islands quickly becoming visible to the primary beam as the angle of incidence is increased from zero. Polar scans at Ni coverages greater than 10 Å show a totally disordered surface, characterized by simply a gradual increase in scattered intensity from glancing incidence to maximum angle of incidence.

IV. CONCLUSION

From measurements of the top-layer atomic composition taken during the deposition of Ni on the Si(111) surface, along with the ICISS scans for surface structure determination, the following room-temperature growth process is proposed. At very low Ni coverages, i.e., ~0.1 Å, Ni atoms diffuse into the Si substrate, locating at predominantly type-*B* $NiSi_2$ lattice sites. At larger coverages, the Ni atoms continue to react with the Si substrate forming three-dimensional islands, with Si atoms comprising the top layer. The silicide islands grow laterally until about 12 Å Ni coverage, at which point they begin to coalesce into a continuous layer. This layer grows in thickness with continued Ni deposition, Si atoms still comprising the top layer, until about 30 Å Ni has been deposited. At this coverage the room-temperature reaction stops and pure Ni layers begin to form.

ACKNOWLEDGMENTS

We especially thank T. M. Buck of AT&T Bell Laboratories for supplying the computer program for the simulation of the ICISS spectra, and J. S. Kraus, also of AT&T Bell Laboratories for supplying drawings of the high-transmission cylindrical electrostatic energy analyzer. This work was supported by the National Science Foundation under Grant No. DMR-8412232.

[1]P. J. Grunthaner, F. J. Grunthaner, A. Madhukar, and J. W. Mayer, J. Vac. Sci. Technol. **19**, 649 (1981).
[2]F. Comin, J. E. Rowe, and P. H. Citrin, Phys. Rev. Lett. **51**, 2402 (1983).
[3]N. W. Cheung and J. W. Mayer, Phys. Rev. Lett. **46**, 671 (1981).
[4]Y. J. Chang and J. L. Erskine, Phys. Rev. B **26**, 4766 (1982).
[5]N. W. Cheung, R. J. Culbertson, L. C. Feldman, P. J. Silverman, K. W. West, and J. W. Mayer, Phys. Rev. Lett. **45**, 120 (1980).
[6]E. J. Van Loenen and J. F. Van Der Veen, Surf. Sci. **157**, 1 (1985).
[7]D. P. Smith, Surf. Sci. **25**, 171 (1971).
[8]M. Aono, Nucl. Instrum. Methods B **2**, 374 (1984).
[9]W. S. Yang, S. C. Wu, and F. Jona, Surf. Sci. **169**, 383 (1986).
[10]R. T. Tung, J. M. Gibson, and J. M. Poate, Phys. Rev. Lett. **50**, 429 (1982).
[11]H. Niehus, Nucl. Instrum. Methods **218**, 230 (1983).
[12]R. Souda, M. Aono, C. Oshima, S. Otani, and Y. Ishizawa, Nucl. Instrum. Methods B **15**, 138 (1986).
[13]J. A. Yarmoff and R. S. Williams, Surf. Sci. **166**, 101 (1986).
[14]W. B. Pearson, *Handbook of Lattice Spacings and Structures of Metals and Alloys* (Pergamon, London, 1958).
[15]C. S. Chang, U. Knipping, and I. S. T. Tsong, Nucl. Instrum. Methods B **18**, 11 (1986).
[16]J. A. Yarmoff, D. M. Cyr, J. H. Huang, S. Kim, and R. S. Williams, Phys. Rev. B **33**, 3856 (1986).
[17]E. J. Van Loenen, A. E. M. J. Fischer, J. F. Van Der Veen, and F. Legones, Surf. Sci. **154**, 52 (1985).
[18]H. H. Brongersma and T. M. Buck, Nucl. Instrum. Methods **132**, 559 (1976).